Biogeosciences, 13, 2339–2352, 2016
www.biogeosciences.net/13/2339/2016/
doi:10.5194/bg-13-2339-2016

Biogeosciences Open Access EGU

Interannual variability of the atmospheric CO_2 growth rate: roles of precipitation and temperature

Jun Wang[1,2], **Ning Zeng**[2,3], **and Meirong Wang**[4]

[1]International Institute for Earth System Science, Nanjing University, Nanjing, China
[2]Institute of Atmospheric Physics, Chinese Academy of Sciences, Beijing, China
[3]Department of Atmospheric and Oceanic Science and Earth System Science Interdisciplinary Center, University of Maryland, College Park, Maryland, USA
[4]Nanjing University of Information Science & Technology, Nanjing, China

Correspondence to: Jun Wang (wangjun@nju.edu.cn)

Received: 10 September 2015 – Published in Biogeosciences Discuss.: 3 December 2015
Revised: 8 March 2016 – Accepted: 4 April 2016 – Published: 21 April 2016

Abstract. The interannual variability (IAV) in atmospheric CO_2 growth rate (CGR) is closely connected with the El Niño–Southern Oscillation. However, sensitivities of CGR to temperature and precipitation remain largely uncertain. This paper analyzed the relationship between Mauna Loa CGR and tropical land climatic elements. We find that Mauna Loa CGR lags precipitation by 4 months with a correlation coefficient of −0.63, leads temperature by 1 month (0.77), and correlates with soil moisture (−0.65) with zero lag. Additionally, precipitation and temperature are highly correlated (−0.66), with precipitation leading by 4–5 months. Regression analysis shows that sensitivities of Mauna Loa CGR to temperature and precipitation are $2.92 \pm 0.20\,\mathrm{PgC\,yr^{-1}\,K^{-1}}$ and $-0.46 \pm 0.07\,\mathrm{PgC\,yr^{-1}}$ $100\,\mathrm{mm^{-1}}$, respectively. Unlike some recent suggestions, these empirical relationships favor neither temperature nor precipitation as the dominant factor of CGR IAV. We further analyzed seven terrestrial carbon cycle models, from the TRENDY project, to study the processes underlying CGR IAV. All models capture well the IAV of tropical land–atmosphere carbon flux (CF_{TA}). Sensitivities of the ensemble mean CF_{TA} to temperature and precipitation are $3.18 \pm 0.11\,\mathrm{PgC\,yr^{-1}\,K^{-1}}$ and $-0.67 \pm 0.04\,\mathrm{PgC\,yr^{-1}}$ $100\,\mathrm{mm^{-1}}$, close to Mauna Loa CGR. Importantly, the models consistently show the variability in net primary productivity (NPP) dominates CGR, rather than heterotrophic respiration. Because previous studies have proved that NPP is largely driven by precipitation in tropics, it suggests a key role of precipitation in CGR IAV despite the higher CGR correlation with temperature. Understanding the relative contribution of CO_2 sensitivity to precipitation and temperature has important implications for future carbon-climate feedback using such "emergent constraint".

1 Introduction

Increasing atmospheric carbon dioxide (CO_2) concentration, from anthropogenic emissions, is the major contributing factor to global warming. This trend can be seen from the long-term CO_2 records from the Mauna Loa Observatory, Hawaii, with a significant seasonal cycle and interannual variability (IAV) superimposed (Keeling et al., 1976, 1995). The IAV of the atmospheric CO_2 growth rate (CGR) is closely connected to the El Niño–Southern Oscillation (ENSO), with noticeable increases during El Niño, and decreases during La Niña events (Bacastow, 1976; Keeling and Revelle, 1985).

The IAV of the atmospheric CGR is the consequence of climate-induced variations in oceanic and terrestrial carbon sources and sinks. Earlier studies have considered the CO_2 flux changes over the oceans, especially the equatorial Pacific Ocean, as the cause of the atmospheric CO_2 IAV (Bacastow, 1976; Francey et al., 1995). However, later inversion modeling studies (Bousquet et al., 2000; Rodenbeck et al., 2003) and many measurement campaigns (Nakazawa et al., 1997; Lee et al., 1998; Feely et al., 2002) have suggested only a small IAV in oceanic carbon uptake. These evidences elucidate the dominant contributions from the terrestrial ecosystems, especially in the tropics, to the IAV of the atmospheric

CGR (Braswell et al., 1997; Bousquet et al., 2000; Zeng et al., 2005a; Qian et al., 2008). Recently, using the combination of land surface models and the satellite-based land cover map, Ahlstrom et al. (2015) pointed out that semi-arid ecosystems, largely occupying low latitudes, dominated the terrestrial carbon interannual variability.

The influence of the ENSO on terrestrial carbon IAV can be largely explained by a "conspiracy" between tropical climatic variations (a tropical-wide drought and warming during El Niño) and the responses of soil and plant physiology (Kinderman et al., 1996; Tian et al., 1998; Knorr et al., 2005; Patra et al., 2005a; Zeng et al., 2005a), as well as some abiotic processes such as fires (van der Werf et al., 2004). However, the processes and strengths of the responses in such terrestrial biotic and abiotic functions remain controversial. Temperature, an important physical variable affecting photosynthesis and respiration, is regarded as the dominant factor on the basis of the significant correlation with Mauna Loa CGR anomalies and in situ observations on tropical tree growth, as well as confirmation by terrestrial carbon cycle models (Kindermann et al., 1996; Braswell et al., 1997; Clark et al., 2003; Cox et al., 2013; Piao et al., 2013; W. Wang et al., 2013; X. Wang et al., 2014). Warming anomalies above a certain threshold can result in a decrease in the terrestrial primary productivity, in part due to the curtailment of the leaf gas exchange (Doughty and Goulden, 2008; Corlett, 2011). Simultaneously, the heterotrophic respiration, R_h, caused by microbial decomposition, increases exponentially with warming temperature (Q_{10}). These direct biological responses to warming temperature variations account for the significant positive correlation between the tropical temperature and CGR (W. Wang et al., 2013; X. Wang et al., 2014). Moreover, further analyses have suggested a two-fold increase in the sensitivity of CGR to the tropical temperature variations in the past 5 decades (X. Wang et al., 2014).

Variation in precipitation over land was proposed as an alternative dominant factor affecting the IAV of the CGR by process-based biogeochemical models of terrestrial ecosystems (Tian et al., 1998; Zeng et al., 2005a; Qian et al., 2008). In order to quantify the individual effects of the ENSO-induced climatic variations, Qian et al. (2008) conducted a series of the sensitivity experiments using a dynamic global vegetation and terrestrial carbon model (VEGAS). They revealed that the contributions from the tropical precipitation and temperature accounted for 56 and 44 % of variations in air–land carbon fluxes during the ENSO events, respectively. In situ records from multiple long-term monitoring plots in the Amazon rainforest have been used to assess the severe drought in 2005, which caused a total biomass carbon loss of 1.2–1.6 Pg (petagrams) (Phillips et al., 2009). Ahlstrom et al. (2015) also found that precipitation and NBP IAV became more correlated with increasing spatial and temporal disaggregation.

These differing viewpoints indicate the current limited understanding of biological processes' response to ENSO. These interannual sensitivities may be important for understanding the strengths of the positive carbon–climate feedback and climate sensitivities of the terrestrial carbon cycle in future climate change (Cox et al., 2000, 2013; Wang et al., 2014; Wenzel et al., 2014). Therefore, in this paper, we again investigate the relationships between Mauna Loa CGR and the tropical climatic variations, based on the up-to-date observations. The tropical climatic parameters are the following: temperature, precipitation, soil moisture, and photosynthetically active radiation (PAR). The performance of IAVs in the tropical terrestrial carbon cycle was simulated by seven state-of-the-art terrestrial carbon cycle models with monthly outputs, from the TRENDY project (Trends in Net Land Atmosphere Carbon Exchanges) (Canadell et al., 2011; Sitch et al., 2015). These mechanistic models are used to delineate the processes underlying the IAVs in CGR, and determine how strong their sensitivities to temperature and precipitation are. In return, these results also give out the evaluations on the 7 terrestrial carbon cycle models on the interannual timescale, which are important for improving them in their development communities.

The paper is organized as follows: Section 2 describes the data sets, methodologies, and terrestrial carbon cycle models that are used. Section 3 presents related results covering three aspects: first, the observed relationships between Mauna Loa CGR and climatic variations; second, the performance and consistencies among the terrestrial carbon cycle models; and third, the climatic sensitivities of CGR and tropical terrestrial carbon cycle. Finally, discussions and concluding remarks are presented in Sect. 4 and 5.

2 Data sets, methodologies, and models

2.1 The observed and reanalysis data sets

The long-term in situ records of atmospheric CO_2 concentrations from the Mauna Loa Observatory were obtained from the website of the National Oceanic and Atmospheric Administration (NOAA) Earth System Research Laboratory (ESRL) (Keeling et al., 1976). We used the monthly mean concentrations to calculate the atmospheric CGR for 1960 to 2012. Meanwhile, we took the globally averaged marine surface monthly mean data from the NOAA for 1980 to 2012 as a comparison with the Mauna Loa data sets (Masarie and Tans, 1995).

The near-surface air temperature and precipitation over land data, with a $0.5^\circ \times 0.5^\circ$ resolution, came from the Climatic Research Unit (CRU) Time-Series (TS) version 3.21 of high resolution gridded data of month-by-month variations in climate (Harris et al., 2014). These data sets were compiled from observations by weather stations around the world, and have been widely used to validate the performance of model simulations in phase 5 of the Coupled Model Intercomparison Project (CMIP5). We took the PAR data from

the NASA Global Energy and Water Exchanges (GEWEX) Surface Radiation Budget (SRB) Release-3.0 data sets, with a $1^\circ \times 1^\circ$ resolution for the period 1984–2007 (Stackhouse et al., 2011). Soil moisture data sets from the Global Land Data Assimilation System Version 2 (GLDAS-2) monthly NOAH model products were adopted, with a $1^\circ \times 1^\circ$ resolution for 1960–2010 (Rodell et al., 2004). We used the sea surface temperature (SST) from the Hadley Center (HadSST2) (Rayner et al., 2005), generated from in situ observations held in the International Comprehensive Ocean–Atmosphere Data Set (ICOADS), to obtain the SST anomalies in the Niño 3.4 regions which refer to the ENSO activities.

2.2 Statistical methods

The CGR was estimated as the difference between the monthly mean concentrations in adjacent years (Patra et al., 2005c; Sarmiento et al., 2010):

$$\mathrm{GR}(t) = CO_2(t+6) - CO_2(t-6), \quad (1)$$

where t denotes the specific month. We then converted the CGR from ppm yr^{-1} into PgC yr^{-1}, based on the conversion factor 1 PgC = 0.471 ppm. The time series of the climatic variables in the tropics (23° S–23° N) over land were area-weighted and averaged. The long-term seasonal cycle was removed from these time series, and in order to precisely extract variations on the interannual timescale, we further applied the Lanczos band-pass filter (Duchon, 1979) with cut-off periods at 12 and 120 months and 121 weights to these time series, which filters out the seasonal cycle and decadal variabilities with 1–10 years window for our analyses.

The relationships between the atmospheric CGR and the climatic variables on an interannual timescale were deciphered via the cross-correlation (Chatfield, 1982):

$$c(k) = \frac{1}{n}\sum_{t=1}^{n} \frac{(X(t)-\overline{X})(Y(t+k)-\overline{Y})}{\sigma(X)\sigma(Y)}, \quad (2)$$

where k denotes the lag months, $\overline{X}$ and $\overline{Y}$ are the means of the time series, and $\sigma(X)$ and $\sigma(Y)$ are the standard deviations. These filtered time series are strongly persistent (or highly auto-correlated), so the effective degrees of freedom (dof) were simply estimated with the approach of Bretherton et al. (1999):

$$\frac{\mathrm{dof}}{n} = \frac{1-r(\Delta t)^2}{1+r(\Delta t)^2}, \quad (3)$$

where n denotes the sample size, $r(\Delta t)$ is the coefficient of the first order autocorrelation, and Δt is 1 month.

Figure 1 shows how the tropical land temperature and precipitation are closely correlated. Cross-correlation analysis indicates that their relationship peaks at a correlation coefficient of −0.66, with a time lag of about 4–5 months in

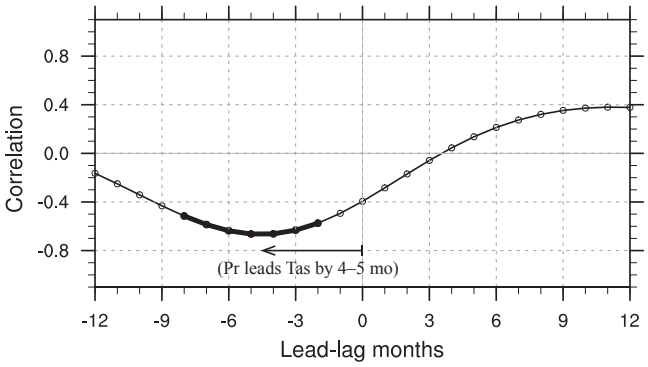

Figure 1. The cross-correlation coefficients between the tropical land precipitation (Pr) and temperature (Tas). The horizontal axis denotes the lead-lag months between precipitation and temperature, with negative values indicating that precipitation leads temperature. Bold line indicates correlation above 95 % significance ($p \leq 0.05$).

temperature. This high correlation coefficient is partly owing to the fact that less land precipitation (for instance during El Niño) can inhibit the evapotranspiration over Tropics, promoting the higher temperature (Zeng et al., 2005a), and also is due to ENSO-related circulation adjustments (Gu and Adler, 2010). Sensitivities of the atmospheric CGR – or tropical land–atmosphere carbon flux (CF_{TA}) – to temperature and precipitation were estimated according to the ridge regression method (Hoerl and Kennard, 2000), the biased estimation for non-orthogonal problems. The linear relationship can be expressed as

$$y(t) = \gamma^{\mathrm{int}} x_{\mathrm{Tas}}(t) + \delta^{\mathrm{int}} x_{\mathrm{Pr}}(t-4) + \varepsilon, \quad (4)$$

where $y(t)$ denotes the IAVs in the Mauna Loa CGR, CF_{TA}, or NPP; x_{Tas} and x_{Pr} denote the IAVs in the tropical land temperature and precipitation; γ^{int} and δ^{int} are the estimated sensitivities by ridge regression; and ε is the residual error. Precipitation leads by 4 months in the regression, according to below analyses. However, these estimated sensitivities only account for the "contributive" effects of temperature and precipitation variations, but not the "true" sensitivities of Mauna Loa CGR, CF_{TA}, or NPP to these variables (Piao et al., 2013). The responses of terrestrial ecosystems to temperature and precipitation are actually nonlinear, so it is difficult to disentangle the individual effects of temperature and precipitation based on the linear statistical method. Additionally, we did not take into consideration the other climatic drivers such as variation in PAR or humidity, which may also contribute to the IAV in atmospheric CGR.

2.3 Terrestrial carbon cycle models and post-processing

In order to understand the contributions of tropical terrestrial ecosystems to the atmospheric CGR and its underlying processes, we used the monthly outputs of seven state-of-the-

art dynamic global vegetation models (DGVMs) that participated in the TRENDY project (TRENDY-v1; Canadell et al., 2011; Sitch et al., 2015). All the DGVMs were forced by observed change in atmospheric CO_2 concentration and historical climate change. The land use was kept time-invariant during the entire S2 simulation. Information on model resolution, nitrogen and fire modules is summarized in Table 1. The models used were (1) CLM4C (Lawrence et al., 2011); (2) CLM4CN (Bonan and Levis, 2010; Lawrence et al., 2011); (3) LPJ (Sitch et al., 2003); (4) LPJ-GUESS (Smith et al., 2001); (5) OCN (Zaehle and Friend, 2010; Zaehle et al., 2010); (6) TRIFFID (Cox, 2001); and (7) VEGAS (Zeng et al., 2005a). Due to the different horizontal resolution of the DGVMs, we interpolated the simulated terrestrial carbon fluxes into a consistent $1^\circ \times 1^\circ$ resolution using the first order conservative remapping scheme (Jones, 1999) following the equation:

$$\overline{F_\mathrm{k}} = \frac{1}{A_\mathrm{k}} \int_{A_\mathrm{k}} f \,\mathrm{d}A, \tag{5}$$

where $\overline{F}_\mathrm{k}$ is the area-averaged destination flux, A_k is the area of cell k, and f is the flux on an old grid which has overlapping area A with the destination grid. After that, the tropical terrestrial carbon fluxes were obtained according to the equation:

$$F = \sum_k \overline{F_\mathrm{k}} A_\mathrm{k}, \tag{6}$$

between 23° S–23° N.

3 Results

3.1 The relationships between the atmospheric CGR and climatic variables

Significant IAV was first detected in the atmospheric CO_2 record at the Mauna Loa Laboratory, Hawaii (Keeling et al., 1995, 1976). Figure 2e presents the long-term IAVs of Mauna Loa CGR during 1960–2012 and the globally averaged marine surface data during 1980–2012. The IAVs of the two data sets are highly consistent, so we mainly focus on the long-term Mauna Loa CGR. Shown in Fig. 2a and e, the standard deviation of Mauna Loa CGR is about 1.03 PgC yr^{-1}, with noticeable increases in the positive anomalies in the Niño 3.4 index, and vice versa for the negative anomalies. The ENSO activities, the dominant year-to-year mode of global climate fluctuations, greatly impact tropical precipitation and temperature on land, through adjustments in atmospheric circulations (Gu and Adler, 2011). Importantly, temperature and precipitation have opposite signs (Fig. 2b and c), with the respective correlation coefficients, relative to the Niño 3.4 index, of 0.55 and -0.83 ($p<0.05$). These ENSO-induced tropical land temperature and precipitation variations contribute to the CF_{TA} in the same direction due to a "conspiracy" between climate anomalies and vegetation–soil response (Qian et al., 2008; Zeng et al., 2005a). For example, warmer and drier conditions during El Niño events can result in the suppression of NPP and enhancement of R_h, both leading to anomalous flux into the atmosphere. However, precipitation does not directly interact with vegetation physiology. Rather, vegetation responds to soil moisture, which is determined not only by precipitation but also by temperature, as higher temperatures lead to increased evaporative water loss (Qian et al., 2008). We also calculated the tropical IAVs in soil moisture from the surface to a 2m depth, and found that the soil moisture decreased during El Niño events, and increased during La Niña events (r of -0.63, with $p = 0.017$ in Fig. 2d). As decreases in soil moisture can suppress NPP and R_h, and vice versa for increases in soil moisture, this may further affect the atmospheric CGR. Besides temperature, precipitation, and soil moisture, other climatic IAVs, such as PAR (Fig. S1 in Supplement), may also influence the variations in terrestrial ecosystems (Nemani et al., 2003).

The coupling between the tropical temperature and precipitation induced by ENSO can be perturbed or interrupted by strong volcanic eruptions, such as those of El Chichón in March 1982 and Mount Pinatubo in June 1991 (Fig. 2). Especially during the post-Pinatubo years, the temperature and precipitation both decreased in the 1991–1992 El Niño events. This unusual relationship resulted from radiative forcing of volcanic sulfate aerosols in the stratosphere (Stenchikov et al., 1998). Meanwhile, there was a hiatus in the coupling between the Niño 3.4 and Mauna Loa CGR in this period. W. Wang et al. (2013) used this decoupling between the Niño 3.4–precipitation–Mauna Loa CGR relationship to highlight the temperature–CO_2 relationship. However, the anomalous growth in vegetation was largely attributed to diffuse light fertilization (Mercado et al., 2009). In general, the canonical ENSO–CGR relationship is robust, although it can occasionally be externally perturbed.

To elucidate the relationship between Mauna Loa CGR and the variations in climatic variables, we conducted cross-correlations of anomalies in Mauna Loa CGR with anomalies in the Niño 3.4 index, tropical surface air temperature, precipitation, soil moisture, and PAR (Fig. 3). We find that ENSO activities generally lead Mauna Loa CGR by about 3–4 months, with a correlation coefficient of 0.70 ($p = 0.007$). The precipitation over land immediately responds to ENSO, and thus also leads Mauna Loa CGR by about 4 months, with a correlation coefficient of -0.63 ($p = 0.016$), similar to the results of W. Wang et al. (2013) (Table 2): this phenomenon may explain the weak correlation of Mauna Loa CGR with concurrent precipitation. However, the temperature over land lags ENSO by about 4 months, suggesting a certain time was needed for surface energy adjustment along with the ENSO-induced circulation and precipitation anomalies (Gu and Adler, 2011). Consequently, the correlation between land

Table 1. Characteristics of the terrestrial carbon cycle models used in this study.

DGVMs	Horizontal resolution	Nitrogen limitation	Fire modules	References
CLM4C	2.5° × 1.875°	No	Yes	Oleson et al. (2010), Lawrence et al. (2011)
CLM4CN	2.5° × 1.875°	Yes	Yes	Bonan and Levis (2010), Lawrence et al. (2011)
LPJ	0.5° × 0.5°	No	Yes	Sitch et al. (2003)
LPJ-GUESS	0.5° × 0.5°	No	Yes	Smith et al. (2001)
OCN	3.75° × 2.5°	Yes	No	Zaehle and Friend (2010), Zaehle et al. (2010)
TRIFFID	3.75° × 2.5°	No	No	Cox (2001)
VEGAS	0.5° × 0.5°	No	Yes	Zeng et al. (2005a)

temperature and Mauna Loa CGR peaks with the correlation coefficient of 0.77 ($p = 0.002$), with a 1-month lag in temperature, a little different from the previous results (W. Wang et al., 2013; X. Wang et al., 2014) (Table 2). This discrepancy in phase implicitly proves that temperature was not the only dominant factor in controlling IAV in atmospheric CGR. The relationship between land precipitation and Mauna Loa CGR can be bridged by the soil moisture. The correlation of Mauna Loa CGR with concurrent soil moisture has the maximum correlation coefficient of -0.65 ($p = 0.022$), suggesting the soil moisture plays an important role in IAV of atmospheric CGR, as analyzed by Qian et al. (2008), though soil moisture is not well constrained by observations. We also show the cross-correlation of Mauna Loa CGR with PAR, but the correlation is not statistically significant.

3.2 Simulations using dynamic global vegetation models

Different from inversion models, process-based terrestrial carbon cycle models can determine the biological dynamics underlying the IAV in atmospheric CGR. Previous studies (Jones et al., 2001; Zeng et al., 2005a; Qian et al., 2008) have analyzed individual models. The TRENDY model output archives provide the opportunity to analyze the mechanisms with an ensemble of state-of-the-art carbon cycle models.

The IAV in ensemble mean tropical CF_{TA}, derived from six state-of-the-art DGVMs, is presented in Fig. 4a with the 1σ inter-model spread and IAV in Mauna Loa CGR. We excluded the CLM4CN to calculate the ensemble mean because of its different response of CF_{TA} and NPP to temperature and precipitation, according to our analyses. The co-variation coefficient, 0.79 with $p = 0.003$, indicates first, that the tropical terrestrial ecosystems dominate the IAV in atmospheric CGR, confirming previous findings (Braswell et al., 1997; Bousquet et al., 2000; Zeng et al., 2005a); and second, that these state-of-the-art DGVMs have the capacity for capturing the historical IAV in terrestrial ecosystems. There is also a significant inconsistency during the post-Pinatubo period 1991–1992, owing to diffuse light fertilization (Mercado et al., 2009). To better understand the contribution from other regions, we also show the IAVs in carbon fluxes for the Northern Hemisphere (23–90° N) and Southern Hemisphere (60–23° S) (Fig. S2). It is clear that the magnitudes of IAVs in carbon fluxes from the Northern Hemisphere ($\sigma = 0.38\,\mathrm{PgC\,yr^{-1}}$) and Southern Hemisphere ($0.21\,\mathrm{PgC\,yr^{-1}}$) are much weaker than the tropical CF_{TA} ($1.03\,\mathrm{PgC\,yr^{-1}}$). Further, the correlations between the variations in carbon fluxes from the extratropical regions and Mauna Loa CGR are insignificant, suggesting that these IAVs may not be caused by ENSO. Therefore, we will only focus on the tropical CF_{TA} below.

The net land–atmosphere carbon flux CF_{TA} results from carbon adjustments in many biotic and abiotic processes. It can be decomposed as

$$CF_{TA} = R_h - NPP + D, \quad (7)$$

where D denotes the disturbances, mainly caused by fires here. We decomposed the simulated ensemble CF_{TA} into three terms ($-$NPP, R_h, and D; Fig. 4b–d), to understand which process was the major factor. (To be precise, we obtained the term D as the residual according to Eq. (7), because it was not explicitly provided in the S2 simulation). We find that the $-$NPP has the strongest magnitude in the IAVs ($0.99\,\mathrm{PgC\,yr^{-1}}$, Table 3) among these three processes. The correlation coefficient of $-$NPP with CF_{TA} reaches 0.97 ($p<0.0001$, Table 3), explaining about 94 % of variance. The standard deviations of R_h and D are 0.29 and $0.10\,\mathrm{PgC\,yr^{-1}}$ (Table 3), respectively, and their correlation coefficients with CF_{TA} are -0.02 ($p = 0.94$) and 0.76 ($p = 0.001$). The weaker IAVs and insignificant correlation of R_h with CF_{TA} may arise from the opposing effects of temperature and precipitation. For example, higher temperatures can enhance R_h, whereas less precipitation – drier conditions – can suppress it. This result agrees with the C^4MIP results in which NPP also dominates CF_{TA} (Fig. S3). In contrast, the weakest term (D) has the very significant correlation with CF_{TA} (Table 3) because both higher temperature and less precipitation promote fires. In summary, the IAV in tropical NPP largely accounts for tropical CF_{TA} variation, dominating the IAV in atmospheric CGR. Because NPP is mainly driven by precipitation (Zeng et al., 2005a; Qian et al., 2008), this suggests precipitation plays an important role in CGR IAV.

Table 2. Summary of previous studies of the relationships between Mauna Loa CGR and climatic variables.

Studies	Correlations of Mauna Loa CGR with climatic variables			
	Temperature	Lead-lag[a]	Precipitation	Lead-lag
W. Wang et al. (2013)	0.70	0	−0.50	−6
X. Wang et al. (2014)	0.53	0	−0.19[b]	–
in this paper	0.77	1	−0.63	−4

[a] Lead-lag months between Mauna Loa CGR and climatic variables. Positive values indicate the climatic variables lag Mauna Loa CGR. [b] This insignificant correlation coefficient was obtained with concurrent precipitation in X. Wang et al. (2014).

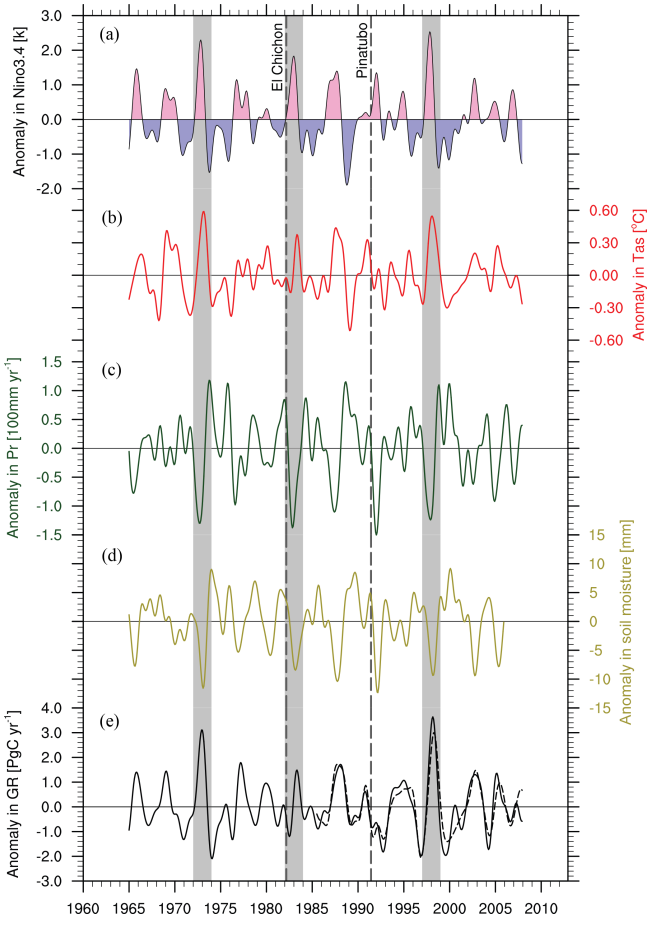

Figure 2. Interannual variabilities (IAVs) in the Niño 3.4 index, tropical land surface air temperature, precipitation, and soil moisture, and atmospheric CO_2 growth rate (CGR). The soil moisture was calculated from the surface layer to a 2 m depth. The atmospheric CGR, for the Scripps Mauna Loa CO_2 data from 1960 to 2012 (solid line) and the globally averaged marine surface CO_2 data from 1980 to 2012 (dashed line), are shown as the difference between the monthly averaged concentrations in the adjacent 2 years. The gray bars represent the three strongest El Niño events during 1965–1966, 1982–1983, and 1997–1998 years and vertical dashed lines show the eruptions of El Chichón and Mount Pinatubo volcanoes in 1982 and 1991, respectively.

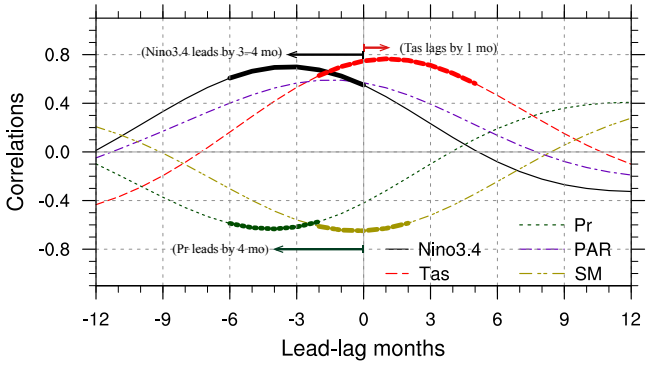

Figure 3. The cross-correlations of anomalies in Mauna Loa CGR with anomalies in the Niño 3.4 index, tropical terrestrial surface air temperature (Tas), precipitation (Pr), soil moisture (SM), and photosynthetically active radiation (PAR). The horizontal axis shows the lead-lag months between them. Negative month values indicate the anomalies in Mauna Loa CGR lag behind. Bold lines indicate correlation above 95 % significance ($p \leq 0.05$), estimated by the effective degree of freedom.

Table 3. Standard deviations of the terrestrial carbon cycle processes.

DGVMs	Standard deviations (PgC yr^{-1})			
	CF_{TA}	−NPP (r[a])	R_h (r)	D (r)
CLM4C	1.73	1.49(0.97)	0.56(0.00)	0.37(0.79)
CLM4CN	1.54	1.33(0.94)	0.60(0.06)	0.33(0.77)
LPJ	0.90	1.05(0.92)	0.40(−0.04)	0.08(−0.54)
LPJ-GUESS	0.84	0.58(0.93)	0.33(0.34)	0.27(0.69)
OCN	0.70	0.72(0.94)	0.25(0.11)	0.01(−0.10)
TRIFFID	1.62	1.34(0.97)	0.45(0.71)	0.00(−0.28)
VEGAS	0.79	1.05(0.95)	0.45(−0.61)	0.08(0.81)
ENS[b]	1.03	0.99(0.97)	0.29(−0.02)	0.10(0.76)
Mauna Loa CGR	1.03[c]	–	–	–

[a] It shows the correlation coefficient with CF_{TA}. [b] The ensemble means were calculated excluding the CLM4CN data because of its large discrepancies responding to temperature and precipitation. [c] This value denotes the standard deviation of Mauna Loa CGR, as a reference to the simulated tropical CF_{TA}.

Though the ensemble tropical CF_{TA} (and −NPP) can well explain the historical IAV in atmospheric CGR, it is necessary to understand the performance of each individual DGVM. Figure 5 shows the color-coded correlation matrices

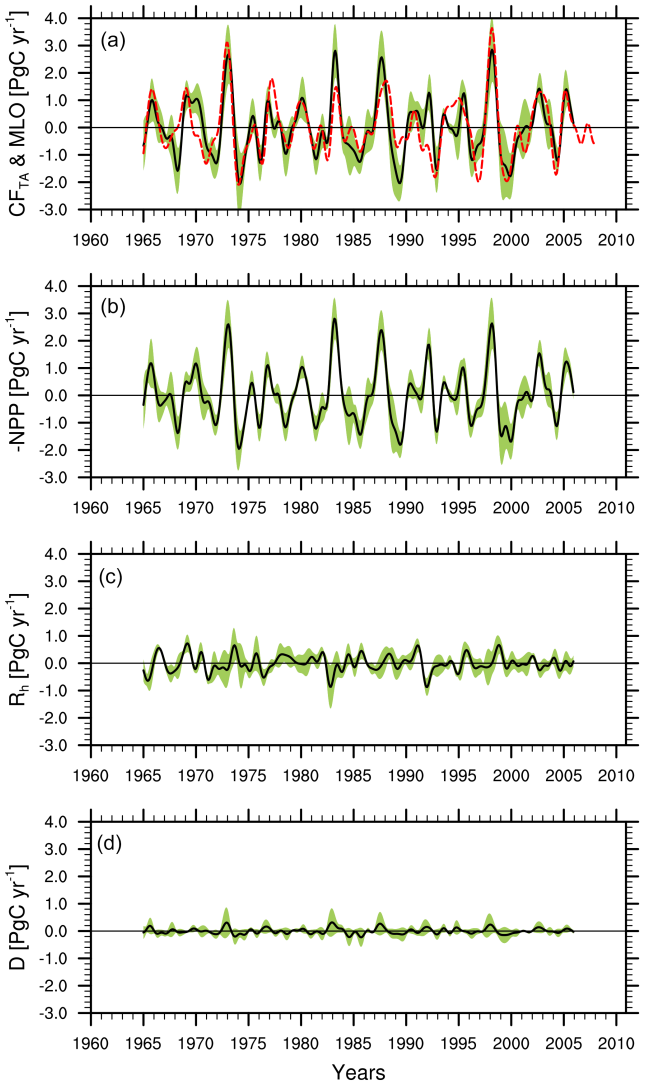

Figure 4. The simulated IAVs of tropical land–atmosphere carbon flux (CF_{TA}), reversed net primary productivity ($-$NPP), heterotrophic respiration (R_h), and disturbances (D) by the seven terrestrial carbon cycle models, involved in the TRENDY project. The solid black lines in the figures denote the ensemble means (excluding CLM4CN), bounded by the 1σ inter-model spread (green shaded areas). The observed IAVs of Mauna Loa CGR from 1960 to 2012 are also shown in **(a)** as a red dashed line. We reversed the NPP in order to make the sign consistent, positive values indicate carbon release from the terrestrial ecosystems.

for the interannual anomalies in the tropical CF_{TA} and $-$NPP estimated by the 7 DGVMs, as well as Mauna Loa CGR and ensemble mean results ("ENS"). As expected, each correlation in pairs among the tropical CF_{TA} is statistically significant ($p<0.03$, Fig. 5a), indicating that these seven DGVMs have great consistency in simulating the IAV in tropical terrestrial ecosystems under the same climatic forcing, although their considerations and parameterizations on the biotic and abiotic processes differ. Moreover, this consistency also suggests the ensemble result is not fortuitous, and well represents the individual DGVM. Therefore, all the correlations of Mauna Loa CGR with the CF_{TA} simulated by each DGVM are significant ($p<0.02$), like the ensemble CF_{TA}. But it is interesting that the correlation coefficients of Mauna Loa CGR with CLM4CN (0.64, $p = 0.02$) and OCN (0.61, $p = 0.01$) are weaker compared to the other models. We notice that the correlations of these two models with the other models in pairs are the weakest. These two DGVMs share a common feature, as both take the nitrogen limitation for the plant growth into consideration (Table 1). Though accounting for these factors suggests these models are more complete in structure, they do not produce better simulations, indicating that the impact of nitrogen on the carbon cycle remains uncertain.

The correlation coefficients in pairs for NPP also show high consistency (Fig. 5b), further confirming the conclusion that the IAV in NPP domination of the CF_{TA} variation is common to all DGVMs. On the contrary, there are discrepancies in the variations of the simulated R_h and D (Fig. S4). Specifically, we find that four (CLM4C, CLM4CN, LPJ, and LPJ-GUESS) have consistent variations in estimated R_h, whereas the others (OCN, TRIFFID, and VEGAS) are different (Fig. S4a). All the simulated R_h, except TRIFFID and VEGAS have insignificant correlation with Mauna Loa CGR, like the behavior of the ensemble mean. Even if the correlations are significant in TRIFFID and VEGAS, they have opposite behaviors (TRIFFID: 0.64, $p = 0.01$; VEGAS: -0.52, $p = 0.08$). The various responses to temperature and precipitation result in the occurrence of large uncertainties in the simulated R_h. It is even more difficult to explain the disturbance term D (Fig. S4b). However, although large uncertainties exist in R_h and D, we still conclude with confidence that the variations in tropical vegetation on the interannual timescale largely account for the atmospheric CGR variability, because the variation magnitudes of R_h and D are much smaller.

Although the correlations of Mauna Loa CGR with the concurrent individual simulated CF_{TA} are all statistically significant (Fig. 5a), the cross-correlations of Mauna Loa CGR with CF_{TA} show that small discrepancies in phase exist among seven DGVMs (Fig. 6a), and of course, are associated with NPP (Fig. 7a). Nevertheless, the correlations of Mauna Loa CGR with the concurrent ensemble CF_{TA} and $-$NPP have maximum values, indicating the multi-model simulated ensemble tropical CF_{TA} and $-$NPP well represent the variations in Mauna Loa CGR. Of course, the small discrepancies in phase of the individual models originate from their different responses to temperature and precipitation. The correlation of ensemble CF_{TA} with temperature peaks at 0.91, without a time lag (Fig. 6b, Table 4), while the correlation between $-$NPP and temperature peaks at 0.82, with around a 1-month lag in temperature (Fig. 7b, Table 4). On the other hand, the correlations of the ensemble CF_{TA} and $-$NPP with precipitation peak at -0.81 and -0.86 with time lags of 4

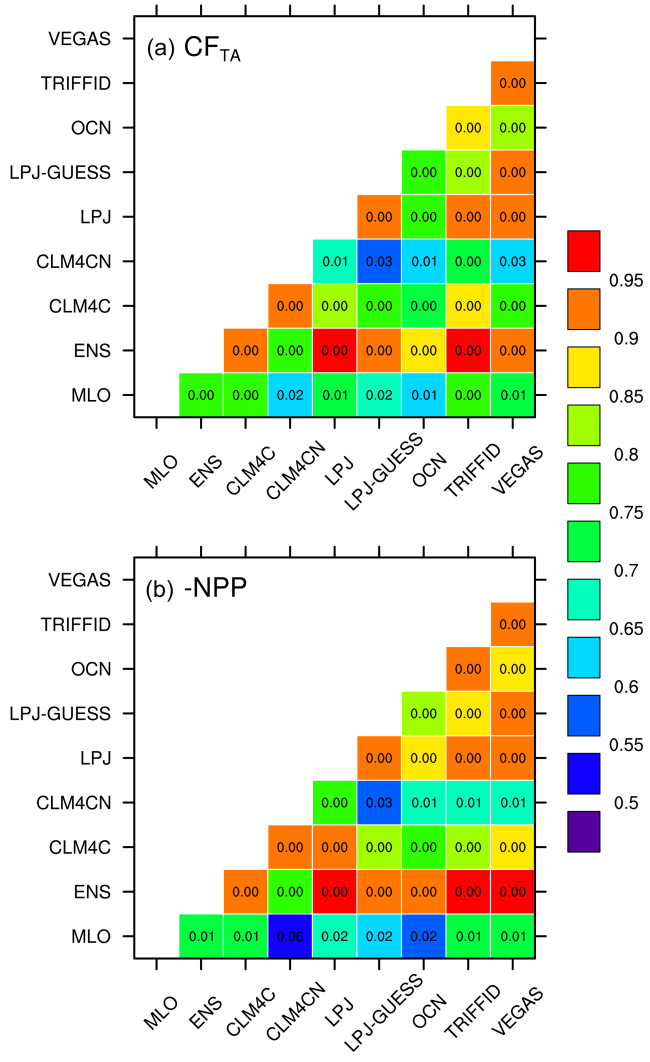

Figure 5. Color-coded correlation matrices for the interannual anomalies in the tropical CF_{TA} and $-$NPP estimated by the seven terrestrial carbon cycle models. Panel **(a)** shows correlation coefficients in pairs among the estimated CF_{TA}, and **(b)** correlation coefficients in pairs among $-$NPP in the period 1960–2010. Mauna Loa CGR and modeled ensemble mean (ENS) are included in these correlations as well. The values in each cell demonstrate the significance levels ($p \leq 0.05$ refers to above 95 % significance).

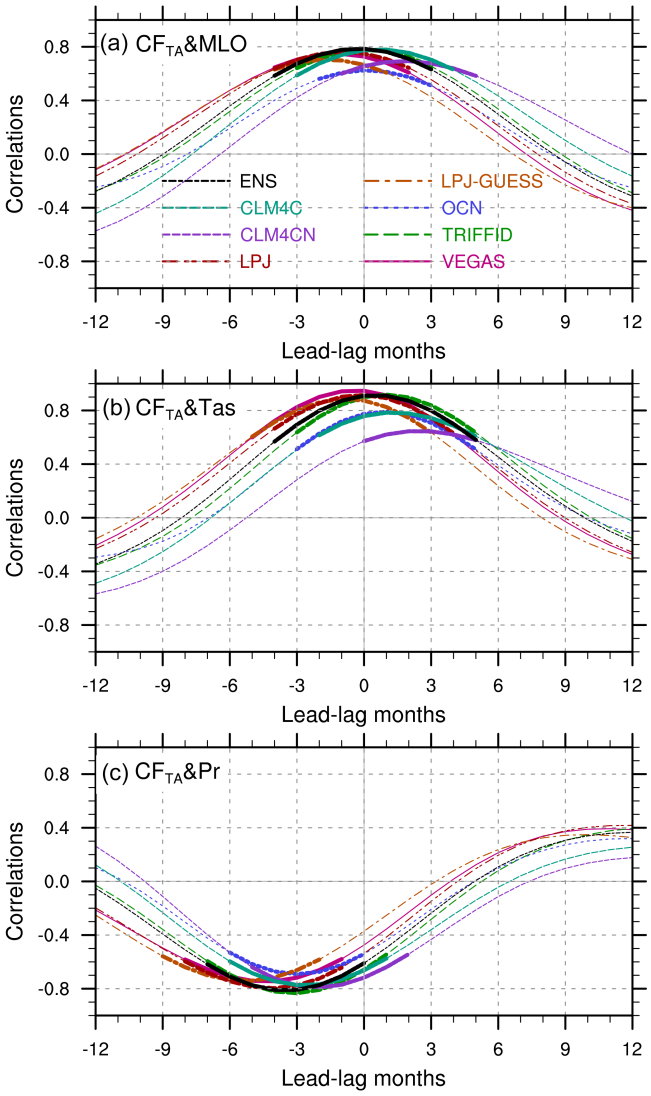

Figure 6. The cross-correlations of the simulated tropical CF_{TA} anomalies with Mauna Loa CGR, tropical near-surface temperature, and precipitation over land. The negative months on the horizontal axis indicate that the anomalies in CF_{TA} lag behind. Bold lines indicate correlation above 95 % significance ($p \leq 0.05$).

and 3 months (Figs. 6c and 7c, Table 4). These behaviors are highly consistent with those in Mauna Loa CGR (Fig. 3). The responses of each DGVM to temperature and precipitation are listed in Table 4. Though there are small discrepancies in phase, their behaviors are similar to each other, except for the CLM4CN model. The responses of CF_{TA} and NPP in CLM4CN to precipitation are too immediate, possibly indicating that the soil moisture adjusts too quickly along with precipitation changes. Unlike NPP, the responses of R_h and D to temperature and precipitation are not so consistent among the models (Figs. S5 and S6), resulting in the discrepancies shown in Fig. S4.

3.3 Sensitivities to temperature and precipitation

As discussed above (Fig. 3), the variations in atmospheric CGR are correlated with the variations in temperature and precipitation induced by ENSO. Simulations by the process-based terrestrial carbon cycle models have demonstrated that the tropical CF_{TA} variability, dominated by the plant primary productivity process, largely accounts for the variations in atmospheric CGR. It further confirms the key importance in precipitation. But quantitatively how sensitive is the atmo-

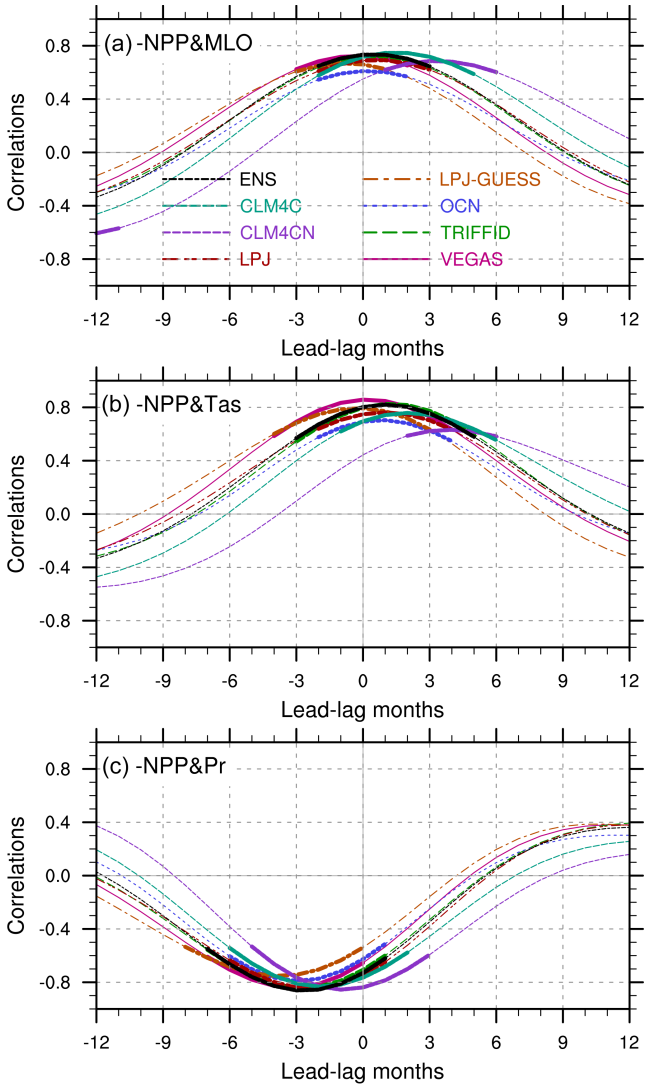

Figure 7. The cross-correlations of −NPP with Mauna Loa CGR, tropical near-surface temperature, and precipitation over land. The negative months on the horizontal axis indicate that the anomalies in −NPP lag behind. Bold lines indicate correlation above 95 % significance ($p \leq 0.05$).

spheric CGR (CF_{TA} / NPP) to temperature and precipitation, respectively? Currently, there is no direct observational evidence. Therefore, for simplicity, we took the ridge regression (Hoerl and Kennard, 2000) to linearly decompose the variations in atmospheric CGR, CF_{TA}, and NPP into two parts, as per Eq. (4). Simultaneously, as the precipitation is not a direct forcing to the terrestrial ecosystems in the models, it usually leads the Mauna Loa CGR by about 4 months (Fig. 3). The precipitation also leads the tropical CF_{TA} and reversed NPP simulated by the DGVMs for about 3–4 months (Table 4). To be consistent, we chose a 4-month lead, to use precipitation as an explanatory variable. The other explanatory variable was the concurrent temperature, owing to its direct impact. We excluded the CLM4CN simulations, because of the model's differing responses to temperature and precipitation (Figs. 6 and 7).

Table 4. The maximum correlations of the simulated tropical terrestrial carbon cycle variability with temperature and precipitation. Lead-lag months between the carbon cycle variability and climatic variables are given in brackets. Positive values indicate that climatic variables lag behind.

DGVMs	Tropical CF_{TA} (Mauna Loa CGR)		Tropical −NPP	
	temperature	precipitation	temperature	precipitation
CLM4C	0.78(1)	−0.77(−3)	0.76(2)	−0.83(−2)
CLM4CN	0.64(2)	−0.79(−2)	0.63(4)	−0.86(−1)
LPJ	0.92(0)	−0.80(−4)	0.76(1)	−0.85(−4)
LPJ-GUESS	0.89(−1)	−0.74(−5)	0.79(0)	−0.75(−3)
OCN	0.79(1)	−0.69(−3)	0.70(1)	−0.79(−3)
TRIFFID	0.92(1)	−0.83(−3)	0.83(1)	−0.84(−3)
VEGAS	0.95(0)	−0.74(−4)	0.86(0)	−0.84(−3)
ENS	0.91(0)	−0.81(−4)	0.82(1)	−0.86(−3)
Mauna Loa CGR	0.77(1)	−0.63(−4)	–	–

The sensitivity of Mauna Loa CGR to the tropical temperature IAV is about $2.92 \pm 0.20\,PgC\,yr^{-1}\,K^{-1}$ (Fig. 8a). This positive response is weaker than that found by Piao et al. (2013) who obtained the contributive effect of temperature variations on residual land sink (RLS, Le Quèrè, 2009) of about $-3.9 \pm 1.1\,PgC\,yr^{-1}\,K^{-1}$ (the negative sign is because of the opposite variability between Mauna Loa CGR and RLS) using multiple linear regression on the global scale. The IAV in the RLS like Mauna Loa CGR is basically determined by the tropical terrestrial ecosystems. Considering the inhomogeneity of temperature variations on the global scale, it is more reasonable to use the tropical temperature variability to estimate their temperature-dependence. The sensitivity of the ensemble tropical CF_{TA} to the temperature variability is about $3.18 \pm 0.11\,PgC\,yr^{-1}\,K^{-1}$, very close to the sensitivity of Mauna Loa CGR. The sensitivities of the tropical CF_{TA} in the individual DGVMs are all positive, ranging from $1.95 \pm 0.12\,PgC\,yr^{-1}\,K^{-1}$ in the OCN model, to $4.78 \pm 0.17\,PgC\,yr^{-1}\,K^{-1}$ in TRIFFID. Three models well simulate this sensitivity: LPJ is 2.88 ± 0.09; LPJ-GUESS is 2.79 ± 0.12; and VEGAS is $2.98 \pm 0.08\,PgC\,yr^{-1}\,K^{-1}$. These CF_{TA} sensitivities are linearly correlated with those of −NPP with a slope of 0.61, and a correlation coefficient of 0.83 ($p < 0.05$), in accord with the conclusion that variabilities in vegetation primary production dominate the CF_{TA} variabilities. This is in accord with the result in Piao et al. (2013), that the response of gross primary production (GPP) to temperature accounts for the response of net biosphere production (NBP).

On the other hand, the sensitivity of Mauna Loa CGR to the tropical precipitation IAV has a value of $-0.46 \pm 0.07\,PgC\,yr^{-1}\,100\,mm^{-1}$ (Fig. 8b). However, Piao et al. (2013) showed that the correlation between RLS and precipitation was not statistically significant with a

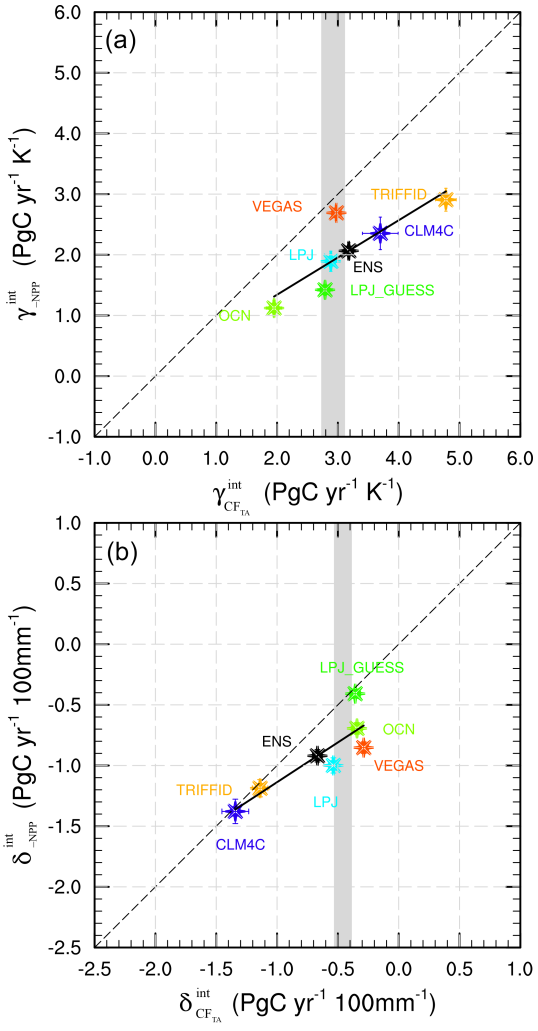

Figure 8. Sensitivities of the tropical anomalies in CF_{TA}, $-NPP$, and Mauna Loa CGR to **(a)** interannual variability in tropical near-surface temperature over land ($PgC\,yr^{-1}\,K^{-1}$) and **(b)** interannual variability in tropical precipitation over land ($PgC\,yr^{-1}\,100\,mm^{-1}$) in 1960–2010. The grey areas show the values of the sensitivities of Mauna Loa CGR with standard errors. Error bars indicate the standard errors of the estimated sensitivities for each model.

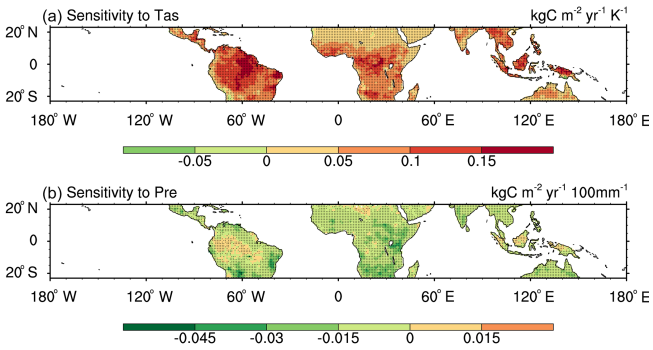

Figure 9. Spatial sensitivities of the ensemble mean in tropical CF_{TA} interannual anomalies to tropical near-surface air temperature ($kgC\,m^{-2}\,yr^{-1}\,K^{-1}$) and precipitation ($kgC\,m^{-2}\,yr^{-1}\,100\,mm^{-1}$) over land. The dotted areas in both figures indicate correlation above 95 % significance ($p \leq 0.05$).

value of $0.8 \pm 1.1\,PgC\,yr^{-1}\ 100\,mm^{-1}$. This difference is mainly due to the usage of (a) annually averaged RLS and precipitation, and (b) globally averaged precipitation variability. The sensitivity of the ensemble tropical CF_{TA} simulated by the DGVMs to precipitation variability is $-0.67 \pm 0.04\,PgC\,yr^{-1}\ 100\,mm^{-1}$, a little stronger than the estimation in Mauna Loa CGR. In the individual DGVMs, three have values within the uncertainty of Mauna Loa CGR: LPJ at -0.54 ± 0.04; LPJ-GUESS at -0.36 ± 0.04; and OCN at $-0.34 \pm 0.05\,PgC\,yr^{-1}\ 100\,mm^{-1}$. The estimation in VEGAS is a little weaker, with a value of $-0.29 \pm 0.03\ PgC\,yr^{-1}\ 100\,mm^{-1}$, whereas the estimations in CLM4C ($-1.34 \pm 0.05\,PgC\,yr^{-1}\ 100\,mm^{-1}$) and TRIFFID ($-1.14 \pm 0.06\,PgC\,yr^{-1}\ 100\,mm^{-1}$) are too strong. Clearly, a significant linear relationship also exists between these sensitivities in CFTA and $-NPP$, with a slope of 0.65, and correlation coefficient 0.86, with $p < 0.05$.

Based on the combination of sensitivities to temperature and precipitation, CLM4C and TRIFFID are more sensitive to these climatic variabilities than the other DGVMs, resulting in a stronger IAVs in these two models (CLM4C: $\sigma = 1.73\,PgC\,yr^{-1}$, TRIFFID: $\sigma = 1.62\,PgC\,yr^{-1}$; Table 3), whereas the other DGVMs have more reasonable magnitudes except CLM4CN (Table 3). Overall, the models simulate well the historical IAV, due to their reasonable sensitivity to the tropical terrestrial ecosystems' temperature and precipitation.

Past studies on the interannual CO_2 variability have mostly focused on the sensitivities of the aggregated carbon flux to temperature and precipitation (Zeng et al., 2005a; Qian et al., 2008; W. Wang et al., 2013). Here we present the sensitivities of the ensemble CF_{TA} grid by grid to temperature and precipitation, in order to roughly have an insight into the regional responses (Fig. 9). The sensitivities to temperature in the tropics are all positive, with remarkably stronger responses in the regions of dense vegetation, especially in the Amazon (Fig. 9a). The African savannas and South Asian forests are weaker with a response of about 0.05–$0.15\,kgC\,m^{-2}\,yr^{-1}\,K^{-1}$. Correspondingly, the sensitivity to precipitation in the tropics is negative for models, except for some regions with insignificant values (Fig. 9b). But interestingly the sensitivities over the African savannas are stronger than those in the Amazon, suggesting that grasses (or shrubs) are more sensitive to precipitation than forests, perhaps because they are more closely associated with the surface soil moisture which is more sensitive to rainfall. However, it is difficult to validate such fine details in the models due to lack of observations.

4 Discussion

In this study, after taking the lag effect of precipitation into consideration (Qian et al., 2008), we find that Mauna Loa CGR has a high correlation coefficient with precipitation ($r = -0.63$), which is only slightly different from the correlation coefficient with temperature ($r = 0.77$). It contrasts with the result of X. Wang et al. (2014). Simultaneously, given that tropical land precipitation and air temperature are dynamically correlated (Fig. 1), we think these correlation coefficients favor neither temperature nor precipitation as the dominant factor of CGR IAV. It contrasts with the result of W. Wang et al. (2013) that is based on the high correlation coefficient between Mauna Loa CGR and temperature. Further, they pointed out that the temperature-CO_2 coupling is mainly owing to the additive responses of NPP and R_h to temperature, while the weaker precipitation-CO_2 coupling is because of the subtractive responses of NPP and R_h to precipitation. However, in this study, the biological dynamics underlying CGR IAV, based on seven DGVMs, reveal that NPP is the dominant process, and R_h variability is obviously weaker, caused by the opposing effects of precipitation and temperature. In the tropics, NPP turned out to be largely driven by precipitation through process-based terrestrial ecosystem models (Zeng et al., 2005a; Qian et al., 2008), indicating the key role of precipitation in CGR IAV. These mechanistic analyses may give out more convincing explanations than the correlation coefficients. Conversely, if NPP dominates the atmospheric CGR, or in other words, precipitation dominates the atmospheric CGR, why does Mauna Loa CGR have a high (or even higher) correlation coefficient with tropical land temperature (than tropical precipitation) (Fig. 3)? This possibly can be explained in part by the high correlation coefficient between the tropical land precipitation and temperature (Fig. 1). On the other hand, R_h and D, though with smaller contributions, can still influence their correlation coefficient (Table 4). Also, we should be cautious of the method for separating the roles of temperature and precipitation in CGR IAV used in this paper and previous studies (Piao et al., 2013; W. Wang et al., 2013; X. Wang et al., 2014). These statistical methods are based on linear decompositions, which may miss important nonlinearities in the physical and biological systems, and cannot accurately deal with the correlations between precipitation and temperature. Therefore, the separate sensitivities of temperature and precipitation diagnosed by these statistical methods are only as the contributive effects (Piao et al., 2013). A better estimation of the contributions of temperature and precipitation should use simulations of processed-based terrestrial carbon cycle models via several sensitivity experiments, while recognizing major uncertainties in the current generation of carbon cycle models.

Although we find that the majority of seven DGVMs can well simulate the IAV in tropical terrestrial ecosystems, the discrepancies in the R_h simulations (Fig. S4) reveal that the soil carbon decomposition processes and microbial activities are not yet to be fully understood. Previous studies (Zeng et al., 2005a; Qian et al., 2008; W. Wang et al., 2013) found that R_h contributes in the same direction of NPP to the IAV of the atmospheric CGR. However, in this study the model ensemble R_h is weaker and not significantly correlated with Mauna Loa CGR.

Besides the tropical NPP and R_h, which is the main focus of our analyses, the atmospheric CGR IAV may also have contributions from other processes or regions, such as variability of the terrestrial carbon flux at mid–high latitude, air–sea carbon fluxes, and the fluxes caused by fire events and land use. Though variabilities of carbon fluxes from the Northern and Southern hemispheres are weak (Fig. S2), some severe events may also modify the canonical tropically-dominated ENSO response. For instance, the anomalous carbon release from 1998 to 2002 across the Northern Hemisphere's mid-latitude regions originated from decreased biological productivity ($0.9\,\mathrm{PgC\,yr^{-1}}$) and forests wildfires, induced by drought and warming (Balzter et al., 2005; Jones and Cox, 2005; Zeng et al., 2005b). The Ocean, another important carbon sink, has a moderate sea-air carbon flux variability of about $\pm 0.5\,\mathrm{PgC\,yr^{-1}}$, dominated over by equatorial Pacific Ocean (Bousquet et al., 2000; McKinley et al., 2004; Patra et al., 2005b; Le Quèrè, 2009). However, during El Niño events, the ocean acts as a sink of atmospheric CO_2, owing to the decrease in equatorial Pacific outgassing caused by the weakened upwelling within the carbon-rich deep water; the opposite occurs during La Niña (Jones et al., 2001; McKinley et al., 2004). This variability opposes that of the atmospheric CGR. Fires also play an important role in the atmospheric CO_2 variability. During the 1997–1998 El Niño event, a fire emissions anomaly, triggered by widespread drought, was $2.1 \pm 0.8\,\mathrm{PgC}$, or $66 \pm 24\,\%$ of CGR anomaly with a 60 % contribution from the Southeast Asia (van der Werf et al., 2004).

At last, there is a concern on the direct comparison between the non-transported modeled carbon fluxes and CO_2 observations. Patra et al. (2005c) conducted a multiple regression analysis between Mauna Loa CGR and a time-dependent inverse (TDI) modeled flux anomalies over 22 TransCom-3 regions, showing the TDI flux anomalies do not explain the detail features in Mauna Loa CGR without any time lag.

5 Concluding remarks

The IAV in atmospheric CGR is closely connected with ENSO activities, as a consequence of the tropical terrestrial carbon sources and sinks, induced by a "conspiracy" between climate anomalies and the responses of vegetation physiology and soil (Zeng et al., 2005a). Understanding the relative contribution of CO_2 sensitivity to tropical precipitation and temperature variabilities has important implications for

future carbon-climate feedback using such "emergent constraint" proposed by Cox et al. (2013). Therefore, in this paper, we re-examined the relationship between atmospheric CGR and climatic variables (temperature, precipitation, soil moisture, and PAR). Moreover, we used seven DGVMs, all participating in the TRENDY project, to delineate the processes underlying the CGR. We applied ridge regression to statistically disentangle the separate effects of temperature and precipitation on the IAV in CGR. Simultaneously, we can better understand the performance of the individual DGVM from these results. The key results are summarized below.

We find that tropical precipitation and temperature are highly correlated, $r = -0.66$, with precipitation leading temperature by 4–5 months, and both are closely connected with ENSO activities. Mauna Loa CGR lags behind the tropical land precipitation variability by about 4 months ($r = -0.63$), but leads temperature by about 1 month (0.77). However, in contrast to some recent suggestions, we argue that these relationships alone do not strongly favor temperature over precipitation as the leading driving factor of CO_2 IAV, nor vice versa. Further, we find that Mauna Loa CGR coincides with soil moisture (-0.65), which is not only determined by precipitation but also by temperature as higher temperatures increase the evapotranspiration effect.

All seven DGVMs capture well the IAV of tropical CF_{TA}. The ensemble CF_{TA} ($\sigma = 1.03\,\mathrm{PgC\,yr^{-1}}$) is highly correlated with Mauna Loa CGR at $r = 0.79$ ($p = 0.003$). Importantly, the models consistently show that the variability in NPP dominates the CF_{TA} variability, while the responses of soil respiration and fire disturbance are much weaker. The standard deviation in ensemble NPP is $0.99\,\mathrm{PgC\,yr^{-1}}$, and in contrast, they are 0.29 and $0.10\,\mathrm{PgC\,yr^{-1}}$ for ensemble R_h and D respectively. As NPP is largely driven by precipitation (via soil moisture), these state-of-the-art DGVMs suggest a key role of precipitation in the IAV of atmospheric CGR.

The sensitivities of Mauna Loa CGR to temperature and precipitation are $2.92 \pm 0.20\,\mathrm{PgC\,yr^{-1}\,K^{-1}}$ and $-0.46 \pm 0.07\,\mathrm{PgC\,yr^{-1}\,100\,mm^{-1}}$, respectively. Meanwhile, the sensitivities of the ensemble mean tropical CF_{TA} produced by the state-of-the-art DGVMs to temperature and precipitation are $3.18 \pm 0.11\,\mathrm{PgC\,yr^{-1}\,K^{-1}}$ and $-0.67 \pm 0.04\,\mathrm{PgC\,yr^{-1}\,100\,mm^{-1}}$, close to those of Mauna Loa CGR. Spatially, the sensitivities to temperature in the tropics are all positive, with remarkably stronger responses over the dense vegetation regions, especially in the Amazon. The sensitivities to precipitation are all negative, with the strongest responses over the African savannas, indicating that grasses (or shrubs) are more sensitive to precipitation than forests.

Data availability

Mauna Loa and globally averaged marine surface monthly CO_2 records are respectively available at http://www.esrl.noaa.gov/gmd/ccgg/trends/index.html and http:/www.esrl.noaa.gov/gmd/ccgg/trends/global.html. CRU near-surface air temperature and precipitation are accessible from http://browse.ceda.ac.uk/browse/badc/cru/data/cru_ts/cru_ts_3.21. Soil moisture data from GLDAS-2 are accessible at the Goddard Earth Sciences Data and Information Services Center, http://disc.sci.gsfc.nasa.gov/hydrology/data-holdings. Sea surface temperature data set is available at http://hadobs.metoffice.com/hadsst2/data/download.html. Outputs of the state-of-the-art DGVMs are available from the TRENDY Project: http://www-lscedods.cea.fr/invsat/RECCAP/V2/.

The Supplement related to this article is available online at doi:10.5194/bg-13-2339-2016-supplement.

Acknowledgements. We acknowledge the TRENDY DGVM community, as part of the Global Carbon Project, for access to gridded land data. And we also wish to thank the Earth System Research Laboratory for the use of their atmospheric CO_2 data sets, the University of East Anglia Climatic Research Unit for land surface air temperature and precipitation, NASA's Atmospheric Science Data Center for the photosynthetically active radiation data, the Goddard Earth Science Data and Information Services Center for the soil moisture, and the UK Met Office's Hadley Centre for the sea surface temperature. This study was supported by the National Key Technology R&D Program (2014BAC22B05). And Ning Zeng's participation was supported by both NOAA (NA10OAR4310248 and NA09NES4400006) and the NSF (AGS-1129088).

Edited by: A. Rammig

References

Ahlstrom, A., Raupach, M. R., Schurgers, G., Smith, B., Arneth, A., Jung, M., Reichstein, M., Canadell, J. G., Friedlingstein, P., Jain, A. K., Kato, E., Poulter, B., Sitch, S., Stocker, B. D., Viovy, N., Wang, Y. P., Wiltshire, A., Zaehle, S., and Zeng, N.: The dominant role of semi-arid ecosystems in the trend and variability of the land CO_2 sink, Science, 348, 895–899, 2015.

Bacastow, R. B. : Modulation of atmospheric carbon dioxide by the Southern Oscillation, Nature, 261, 116–118, 1976.

Balzter, H., Gerard, F. F., George, C. T., Rowland, C. S., Jupp, T. E., McCallum, I., Shvidenko, A., Nilsson, S., Sukkinin, A., Onuchin, A., and Schmullius, C.: Impact of the Arctic Oscillation pattern on interannual forest fire variability in Central Siberia, Geophys. Res. Lett., 32, L14709, doi:10.1029/2005gl022526, 2005.

Bonan, G. B. and Levis S.: Quantifying carbon-nitrogen feedbacks in the Community Land Model (CLM4), Geophys. Res. Lett., 37, L07401, doi:10.1029/2010GL042430, 2010.

Bousquet, P., Peylin, P., Ciais, P., Le Quèrè, C., Friedlingstein, P., and Tans, P. P.: Regional changes in carbon dioxide fluxes of land and oceans since 1980, Science, 290, 1342–1346, 2000.

Braswell, B. H., Schimel, D. S., Linder, E., and Moore, B.: The response of global terrestrial ecosystems to interannual temperature variability, Science, 278, 870–872, 1997.

Bretherton, C. S., Widmann, M., Dymnikov, V. P., Wallace, J. M., and Blade, I.: The effective number of spatial degrees of freedom of a time-varying field, J. Climate, 12, 1990–2009, 1999.

Canadell, J., Ciais, P., Gurney, K., Le Quèrè, C., Piao, S., Raupach, M. R., and Sabine, C. L.: An international effort to quantify regional C fluxes, EOS, 92, 81–82, 2011.

Chatfield, C.: The analysis of time series: An introduction, Chapman & Hall, London, 1982.

Clark, D. A., Piper, S. C., Keeling, C. D., and Clark, D. B.: Tropical rain forest tree growth and atmospheric carbon dynamics linked to interannual temperature variation during 1984–2000, P. Natl. Acad. Sci. USA, 100, 5852–5857, 2003.

Corlett, R. T.: Impacts of warming on tropical lowland rainforests, Trends Ecol. Evol., 26, 606–613, 2011.

Cox, P. M.: Description of the "TRIFFID" Dynamic Global Vegetation Model, Technical Note 24, HadleyCentre, Met Office, 2001.

Cox, P. M., Betts, R. A., Jones, C. D.,Spall, S. A., and Totterdell, I. J.: Acceleration of global warming due to carbon-cycle feedbacks in a coupled climate model, Nature, 408, 184–187, 2000.

Cox, P. M., Pearson, D., Booth, B. B., Friedlingstein, P., Huntingford, C., Jones, C. D., and Luke, C. M.: Sensitivity of tropical carbon to climate change constrained by carbon dioxide variability, Nature, 494, 341–344, 2013.

Doughty, C. E. and Goulden, M. L.: Are tropical forests near a high temperature threshold?, J. Geophys. Res., 113, G00B07, doi:10.1029/2007jg000632, 2008.

Duchon, C. E.: Lanczos Filtering in One and Two Dimensions, J. Appl. Meteorol., 18, 1016–1022, 1979.

Feely, R. A., Boutin, J., Cosca, C. E., Dandonneau, Y., Etcheto, J., Inoue, H. Y., Ishii, M., Le Quéré, C., Machey, D. J., McPhaden, M., Metzl, N., Poisson, A., and Wanninkhof, R.: Seasonal and interannual variability of CO_2 in the equatorial Pacific, Deep-Sea Res. Pt. I, 49, 2443–2469, 2002.

Francey, R. J., Tans, P. P., Allison, C. E., Enting, I. G., White, J. W. C., and Trolier, M.: Changes in Oceanic and Terrestrial Carbon Uptake since 1982, Nature, 373, 326–330, 1995.

Gu, G. J. and Adler, R. F.: Precipitation and Temperature Variations on the Interannual Time Scale: Assessing the Impact of ENSO and Volcanic Eruptions, J. Climate, 24, 2258–2270, 2011.

Harris, I., Jones, P. D., Osborn, T. J., and Lister, D. H.: Updated high-resolution grids of monthly climatic observations – the CRU TS3.10 Dataset, Int. J. Climatol., 34, 623–642, 2014.

Hoerl, A. E. and Kennard, R. W.: Ridge Regression: Biased Estimation for Nonorthogonal Problems, Technometrics, 42, 80–86, 2000.

Jones, C. D. and Cox P. M.: On the significance of atmospheric CO_2 growth rate anomalies in 2002–2003, Geophys. Res. Lett., 32, L14816, doi:10.1029/2005gl023027, 2005.

Jones, C. D., Collins, M., Cox, P. M., and Spall, S. A.: The carbon cycle response to ENSO: A coupled climate-carbon cycle model study, J. Climate, 14, 4113–4129, 2001.

Jones, P. W.: First- and second-order conservative remapping schemes for grids in spherical coordinates, Mon. Weather Rev., 127, 2204–2210, 1999.

Keeling, C. D. and Revelle, R.: Effects of El-Niño Southern Oscillation on the Atmospheric Content of Carbon-Dioxide, Meteoritics, 20, 437–450, 1985.

Keeling, C. D., Bacastow, R. B., Bainbridge, A. E., Ekdahl, C. A., Guenther, P. R., Waterman, L. S., and Chin, J. F. S.: Atmospheric Carbon-Dioxide Variations at Mauna-Loa Observatory, Hawaii, Tellus, 28, 538–551, 1976.

Keeling, C. D., Whorf, T. P.,Wahlen, M., and van der Plichtt, J.: Interannual extremes in the rate of rise of atmospheric carbon dioxide since 1980, Nature, 375, 666–670, 1995.

Kindermann, J., Würth, G., Kohlmaier, G. H., and Badeck, F. W.: Interannual variation of carbon exchange fluxes in terrestrial ecosystems, Global Biogeochem. Cy., 10, 737–755, 1996.

Knorr, W., Scholze, M., Gobron, N., Pinty, B., and Kaminski, T.: Global-scale drought caused atmospheric CO_2 increase, EOS Archives, 86, 178–181, 2005.

Lawrence, D. M., Oleson, K. W., Flanner, M. G., Thornton, P. E., Swenson, S. C., Lawrence, P. J., Zeng, X. B., Yang, Z. L., Levis, S., Sakaguchi, K., Bonan, G. B., and Slater, A. G.: Parameterization Improvements and Functional and Structural Advances in Version 4 of the Community Land Model, J. Adv. Model. Earth Sy., 3, M03001, doi:10.1029/2011ms000045, 2011.

Lee, K., Wanninkhof, R., Takahashi, T., Doney, S. C., and Feely, R. A.: Low interannual variability in recent oceanic uptake of atmospheric carbon dioxide, Nature, 396, 155–159, 1998.

Le Quèrè, C.: Trends in the sources and sinks of carbon dioxide, Nature Geosci., 2, 831–836, 2009.

Masarie, K. A. and Tans, P. P.: Extension and integration of atmospheric carbon dioxide data into a globally consistent measurement record, J. Geophys. Res., 100, 11593–11610, 1995.

McKinley, G. A., Follows, M. J., and Marshall, J.: Mechanisms of air-sea CO_2 flux variability in the equatorial Pacific and the North Atlantic, Global Biogeochem. Cy., 18, GB2011, doi:10.1029/2003gb002179, 2004.

Mercado, L. M., Bellouin, N., Sitch, S., Boucher, O., Huntingford, C., Wild, M., and Cox, P. M.: Impact of changes in diffuse radiation on the global land carbon sink, Nature, 458, 1014-U1087, doi:10.1038/Nature07949, 2009.

Oleson, K. W., Lawrence, D. M., Gordon, B., Flanner, M. G., Kluzek, E., Peter, J., Levis, S., Swenson, S. C., Thornton E., and Feddema, J.: Technical description of version 4.0 of the Community Land Model (CLM), NCAR/TN-478+STR, 2010.

Nakazawa, T., Morimoto, S., Aoki, S., and Tanaka, M.: Temporal and spatial variations of the carbon isotopic ratio of atmospheric carbon dioxide in the western Pacific region, J. Geophys. Res.-Atmos., 102, 1271–1285, 1997.

Nemani, R. R., Keeling, C. D., Hashimoto, H., Jolly, W. M., Piper, S. C., Tucker, C. J., Myneni, R. B., and Running, S. W.: Climate-driven increases in global terrestrial net primary production from 1982 to 1999, Science, 300, 1560–1563, 2003.

Patra, P. K., Ishizawa, M., Maksyutov, S., Nakazawa, T., and Inoue, G.: Role of biomass burning and climate anomalies for land-atmosphere carbon fluxes based on inverse modeling of atmospheric CO_2, Global Biogeochem. Cy., 19, GB3005, doi:10.1029/2004GB002258, 2005a.

Patra, P. K., Maksyutov, S., Ishizawa, M., Nakazawa, T., Takahashi, T., and Ukita, J.: Interannual and decadal changes in the sea-air CO_2 flux from atmospheric CO_2 inverse modeling, Global Biogeochem. Cy., 19, GB4013, doi:10.1029/2004gb002257, 2005b.

Patra, P. K., Maksyutov, S., and Nakazawa, T.: Analysis of atmospheric CO_2 growth rates at Mauna Loa using CO_2 fluxes derived from an inverse model, Tellus B, 57, 357–365, 2005c.

Phillips, O. L., Aragão, L., Lewis, S. L., Fisher, J. B., Lloyd, J., López-González, G., Malhi, Y., Monteagudo, A., Peacock, J., Quesada, C. A., Heijden, G., Almeida, S., Amaral, I., Arroyo, L., Aymard, G., Baker, T. R., Bánki, O., Blanc, L., Bonal, D., Brando, P., Chave, J., de Oliveira, Á., Cardozo, N., Czimczik, C., Feldpausch, T., Freitas, M. A., Gloor, E., Higuchi, N., Jiménez, E., Lloyd, G., Meir, P., Mendoza, C., Morel, A., Neill, D. A., Nepstad, D., Patiño, S., Peñuela, M. C., Prieto, A., Ramírez, F., Schwarz, M., Silva, J., Silveira, M., Thomas, A. S., Steege, H., Stropp, J., Vásques, R., Zelazowski, P., Dávila, E. A., Andelman, S., Andrade, A., Chao, K. J., Erwin, T., Fiore, A. D., Honorio, E., Keeling, H., Killeen, T. J., Laurance, W. F., Cruz, A. P., Pitman, N. C. A., Vargas, P. N., Ramírez-Angulo, H., Rudas, A., Salamão, R., Silva N., Terborgh, J., and Torres-Lezama, A.: Drought Sensitivity of the Amazon Rainforest, Science, 323, 1344–1347, 2009.

Piao, S. L., Sitch, S., Ciais, P., Friedlingstein, P., Peylin, P., Wang, X. H., Ahlstrom, A., Anav, A., Canadell, J. G., Cong, N., Huntingford, C., Jung, M., Levis, S., Levy, P. E., Li, J. S., Lin, X., Lomas, M. R., Lu, M., Luo, Y. Q., Ma, Y. C., Myneni, R. B., Poulter, B., Sun, Z. Z., Wang, T., Viovy, N., Zaehle, S., and Zeng, N.: Evaluation of terrestrial carbon cycle models for their response to climate variability and to CO_2 trends, Glob. Change Biol., 19, 2117–2132, 2013.

Qian, H., Joseph, R., and Zeng, N.: Response of the terrestrial carbon cycle to the El Niño-Southern Oscillation, Tellus B, 60, 537–550, 2008.

Rayner, N. A., Brohan, P., Parker, D. E., Folland, C. K., Kennedy, J. J., Vanicek, M., Ansell, T. J., and Tett, S. F. B.: Improved Analyses of Changes and Uncertainties in Sea Surface Temperature Measured In Situ since the Mid-Nineteenth Century: The HadSST2 Dataset, J. Climate, 19, 446–469, 2005.

Rodell, M., Houser, P. R., Jambor, U., Gottschalck, J., Mitchell, K., Meng, C. J., Arsenault, K., Cosgrove, B., Radakovich, J., Bosilovich, M., Entin, J. K., Walker, J. P., Lohmann, D., and Toll, D.: The global land data assimilation system, B. Am. Meteorol. Soc., 85, 381–394, 2004.

Rodenbeck, C., Houweling, S., Gloor, M., and Heimann, M.: CO_2 flux history 1982–2001 inferred from atmospheric data using a global inversion of atmospheric transport, Atmos. Chem. Phys., 3, 1919–1964, doi:10.5194/acp-3-1919-2003, 2003.

Sarmiento, J. L., Gloor, M., Gruber, N., Beaulieu, C., Jacobson, A. R., Mikaloff Fletcher, S. E., Pacala, S., and Rodgers, K.: Trends and regional distributions of land and ocean carbon sinks, Biogeosciences, 7, 2351–2367, doi:10.5194/bg-7-2351-2010, 2010.

Sitch, S., Smith, B., Prentice, I. C., Arneth, A., Bondeau, A., Cramer, W., Kaplan, J. O., Levis, S., Lucht, W., Sykes, M. T., Thonicke, K., and Venevsky, S.: Evaluation of ecosystem dynamics, plant geography and terrestrial carbon cycling in the LPJ dynamic global vegetation model, Glob. Change Biol., 9, 161–185, 2003.

Sitch, S., Friedlingstein, P., Gruber, N., Jones, S. D., Murray-Tortarolo, G., Ahlström, A., Doney, S. C., Graven, H., Heinze, C., Huntingford, C., Levis, S., Levy, P. E., Lomas, M., Poulter, B., Viovy, N., Zaehle, S., Zeng, N., Arneth, A., Bonan, G., Bopp, L., Canadell, J. G., Chevallier, F., Ciais, P., Ellis, R., Gloor, M., Peylin, P., Piao, S. L., Le Quéré, C., Smith, B., Zhu, Z., and Myneni, R.: Recent trends and drivers of regional sources and sinks of carbon dioxide, Biogeosciences, 12, 653–679, doi:10.5194/bg-12-653-2015, 2015.

Smith, B., Prentice, I. C., and Sykes, M. T.: Representation of vegetation dynamics in the modelling of terrestrial ecosystems: comparing two contrasting approaches within European climate space, Global Ecol. Biogeogr., 10, 621–637, 2001.

Stackhouse, Jr., Paul, W., Shashi, K. G., Stephen, J. C., Mikovitz, J. C., Zhang, T. P., and Hinkelman, L. M.: The NASA/GEWEX Surface Radiation Budget Release 3.0: 24.5-Year Dataset, GEWEX News, 21 February, 10–12, 2011.

Stenchikov, G. L., Kirchner, I., Robock, A., Graf, H.-F., Antuña, J. C., Grainger, R. G., Lambert, A., and Thomason, L.: Radiative forcing from the 1991 Mount Pinatubo volcanic eruption, J. Geophys. Res., 103, 13837, doi:10.1029/98jd00693, 1998.

Tian, H. Q., Melillo, J. M., Kicklighter, D. W., McGuire, A. D., Helfrich, J. V. K., Moore, B., and Vorosmarty, C. J.: Effect of interannual climate variability on carbon storage in Amazonian ecosystems, Nature, 396, 664–667, 1998.

van der Werf, G. R., Randerson, J. T., Collatz, G. J., Giglio, L., Kasibhatla, P. S., Arellano, A. F., Olsen Jr., S. C., and Kasischke, E. S.: Continental-scale partitioning of fire emissions during the 1997 to 2001 El Niño/La Niña period, Science, 303, 73–76, 2004.

Wang, J., Zeng, N., Liu, Y., and Bao, Q.: To what extent can interannual CO_2 variability constrain carbon cycle sensitivity to climate change in CMIP5 Earth System Models?, Geophys. Res. Lett., 41, 3535–3544, 2014.

Wang, W., Ciais, P., Nemani, R., Canadell, J. G., Piao, S., Sitch, S., White, M. A., Hashimoto, H., Milesi, C., and Myneni R. B.: Variations in atmospheric CO_2 growth rates coupled with tropical temperature, PNAS, 110, 13061–13066, 2013.

Wang, X., Paio, S., Ciais, P., Friedlingstein, P., Myneni, R. B., Cox, P., Heimann, M., Miller, J., Peng, S., Wang, T., Yang, H., and Chen, A.: A two-fold increase of carbon cycle sensitivity to tropical temperature variations, Nature, 506, 212–215, 2014.

Wenzel, S., Cox, P. M., Eyring, V., and Friedlingstein, P.: Emergent constraints on climate-carbon cycle feedbacks in the CMIP5 Earth system models, J. Geophys. Res.-Biogeo., 119, 794–807, 2014.

Zaehle, S. and Friend, A. D.: Carbon and nitrogen cycle dynamics in the O-CN land surface model: 1. Model description, site-scale evaluation, and sensitivity to parameter estimates, Global Biogeochem. Cy., 24, GB1005, doi:10.1029/2009gb003521, 2010.

Zaehle, S., Friend, A. D., Friedlingstein, P., Dentener, F., Peylin, P., and Schulz, M.: Carbon and nitrogen cycle dynamics in the O-CN land surface model: 2. Role of the nitrogen cycle in the historical terrestrial carbon balance, Global Biogeochem. Cy., 24, GB1006, doi:10.1029/2009gb003522, 2010.

Zeng, N., Mariotti, A., and Wetzel, P.: Terrestrial mechanisms of interannual CO_2 variability, Global Biogeochem. Cy., 19, GB1016, doi:10.1029/2004gb002273, 2005a.

Zeng, N., Qian, H. F., Roedenbeck, C., and Heimann, M.: Impact of 1998–2002 midlatitude drought and warming on terrestrial ecosystem and the global carbon cycle, Geophys. Res. Lett., 32, L22709, doi:10.1029/2005gl024607, 2005b.